REVIEW

Editor's Choice

ADVANCED
ENGINEERING
MATERIALS

www.aem-journal.com

A Review of the Factors That Can Increase the Risk of Sulfide Stress Cracking in Thermomechanical Controlled Processed Pipeline Steels

*Sarah Hiew Sze Kei, Willem Maarten van Haaften, T. Ben Britton, and Stella Pedrazzini**

This review aims to improve our understanding of the important factors which influence the susceptibility of thermomechanical controlled processed (TMCP) steels to sulfide stress cracking (SSC). Mechanisms involved in hydrogen embrittlement (HE) from three perspectives are focused on: the microstructure constituents of TMCP steels; environmental factors; and fracture mechanism of SSC. Microstructures are reviewed as they affect the diffusion and trapping of hydrogen that can reduce the resistance to fracture. Environmental factors discussed highlight that when exposed to an aqueous H_2S environment, a sulfide layer can form and influence the ingress of hydrogen, and this is affected by pH, temperature, and H_2S partial pressure. Fracture is influenced by the nature of the crack tip and the crack tip plastic zone during crack propagation, and hydrogen can significantly affect crack tip growth. This review provides a critical assessment of the interplay between these three factors and aims to provide understanding to enhance our engineering approaches to manage and mitigate against fracture of TMCP steels.

1. Background Introduction

Steel pipelines used for oil and gas transportation are mainly manufactured using the Thermomechanical controlled process (TMCP) technology which utilizes thermomechanical rolling

S. Hiew. S. K., T. B. Britton, S. Pedrazzini
Department of Materials
Imperial College London
London, UK
E-mail: s.pedrazzini@imperial.ac.uk

W. M. van Haaften
Shell Global Solutions International B.V.
Amsterdam, The Netherlands

T. B. Britton
Department of Materials Engineering
University of British Columbia
Vancouver, BC, Canada

The ORCID identification number(s) for the author(s) of this article can be found under https://doi.org/10.1002/adem.202300406.

and accelerated cooling with the original aim to produce high-strength low-alloy (HSLA) steel with improved toughness and weldability.[1] However, there is a risk that the exposure of TMCP steel pipelines to a so-called "sour environment", that is, one that contains H_2S, could lead to sulfide stress cracking (SSC). Generally, there are two types of SSCs. Type I SSC also known as stress-orientated hydrogen-induced crack (SOHIC) can be observed in the welded regions of pipeline steels as cracks in a step-like manner perpendicular to surface of the material.[2–5] The more commonly observed type II SSC is found in both the welded regions and parent material of pipeline steel, where the main crack path grows normal to the direction of principal stress.[4,6] Hence, the SSC referred to in this review will focus on the more frequently observed type II.

One mitigating approach can be the use of a more expensive alternative, for example, steel pipeline with corrosion-resistant alloy (CRA) as the cladding layer.[7,8] This has motivated a significant number of studies and the development of standards to evaluate and mitigate the SSC susceptibility of TMCP pipeline steels.[9] This body of work has resulted in a consensus that SSC occurs from the synergistic effect of applied force and hydrogen embrittlement (HE) influenced by the presence of sulfide species of H_2S.[2–4,6,10–12] Hence, this review will discuss the factors influencing the SSC susceptibility in TMCP steels through HE from three perspectives, as shown in **Figure 1**: the microstructure constituents of TMCP; the environmental factors, and the fracture mechanism of SSC.

In order to meet the economical demands of oil and gas industry, there has been an increase in the diameter of pipelines.[13] A common pipe forming process used to achieve a minimum approximate diameter of 406 mm is via the UOE process.[14] Briefly, UOE process involves pressing steel plates manufactured by continuous casting and hot rolling into first a (U) shape, followed by a (O) cylinder, which is then welded and hydrostatically expanded (E) to the final desired shape.[14] To provide focus, and help provide insight into the interplay of factors highlighted in Figure 1, this review will explore microstructural regions within the parent material TMCP steel.

**ADVANCED
SCIENCE NEWS**

www.advancedsciencenews.com

**ADVANCED
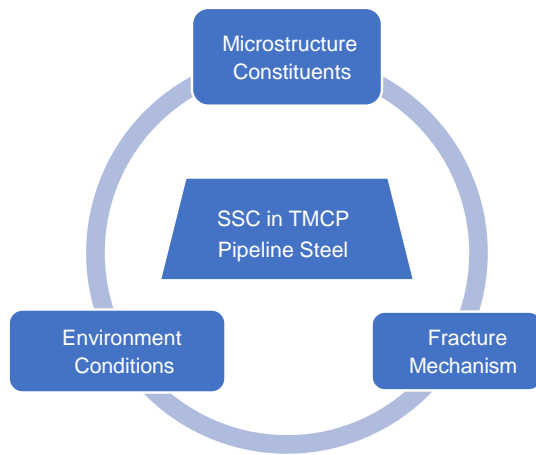ENGINEERING
MATERIALS**

www.aem-journal.com

Figure 1. Schematic shows the three main factors influencing SSC in TMCP pipeline steels.

2. Microstructure Constituents Influencing SSC

2.1. Types of TMCP Microstructures' Constituents

During the cooling of a typical Fe–C alloy solution, the austenite (γ) phase with face-centered-cubic (FCC) structure becomes stable up to the eutectoid temperature of 996.15 K where nucleation of phases such as body-centered-cubic (BCC) ferrite (α-Fe) and cementite (Fe₃C) occurs depending on variables such as the cooling rate, starting carbon content, and alloying elements present.[15] The grains of these initial γ phase formed are known as prior or parent austenite grains (PAGs) and the boundaries of PAG are known to influence the behavior of SSC cracks.[16,17] The initiation and propagation of SSC at these PAG boundaries is not only affected by the size of PAGs or type of element that partitioned to these boundaries, but also the type of microstructure constituent that nucleates from these boundaries.[18–21] Hence, the following sections will highlight and discuss different microstructure constituents of interests within PAG in relevance to their contribution to SSC.

This section will briefly review the types of microstructures of interest commonly found in low-carbon TMCP pipeline steels.

2.1.1. Martensite-Austenite Constituent

Martensite–austenite (M/A) constituent is a mixture of retained austenite (RA) and untempered metastable martensite that can exist as islands or rods as small as 1.5 μm in its longest diameter.[22,23] These hard islands tend to act as initiation sites for SSC but may or may not advance the crack depending on the types of its neighboring microstructural features.[24] Not only are these M/A sites of crack initiations, they are also sites of hydrogen traps due to the raised dislocation density of martensite compared to the neighboring austenite.[25] The distribution of hydrogen within a microstructure may also depend on the existing morphology of M/A. According to Ramachandran et al.,[26] a disordered M/A morphology resulted in ≈35% higher dislocation density when compared to typically observed M/A with alternating lath

MA morphology. Moreover, these disorderly arranged M/A tends to form at the boundaries of PAG, promoting the propagation of SSC along these boundaries.[16,17,26] Furthermore, the induced transformation of RA into martensite can also increase the compressive stress field around the crack tip, leading to crack closure.[27]

2.1.2. Granular Bainite

Generally, bainite is formed at transformation temperatures between that which forms pearlite and martensite to give laths consisting of clusters of ferrite plates surrounded by RA or cementite, resulting in higher toughness but same hardness when compared to martensite.[20] Depending on the start transformation temperature, the rate of diffusion allows for the precipitation of carbon either at the boundaries of ferrite platelets to give upper bainite or within the ferrite platelets to lower bainite.[20] Similarly, another type of bainite such as acicular bainite mainly consists of carbide-free ferrite laths where negligible amounts of martensite exist as either acicular martensite within or between the ferrite laths or as a thin film of M/A constituent between the ferrite.[28] This is because acicular bainite forms at a higher temperature, providing a higher driving force for the diffusion of carbon before it is quenched at a much higher cooling rate than upper or lower bainite, limiting the amount of cementite precipitated.[28] Further discussions regarding the thermodynamics and kinetics of either displacive deformation or reconstructive diffusion-controlled mechanisms or both in the formation of bainite can be found elsewhere.[20,29,30] Acicular bainite as well as upper and lower bainite will also not be discussed in this review and further details can be found elsewhere.[20]

In order to increase the formability of TMCP pipeline, Shinohara et al.[31] was able to achieve a dual-phase microstructure of ferrite and granular bainite utilizing a type of accelerated cooling, that is, mild accelerated cooling, to improve the conventional single bainite microstructure obtained from interrupted direct quenched steel. This helps to improve the strain hardening rate of the material while maintaining a yield-to-ultimate tensile strength (Y/T) ratio of not more than 0.93 which is required according to API 5L standard.[32] This dual-phase microstructure is advantageous especially in increasing the buckling resistance in pipeline steel to withstand high strain and operational pressure levels of ground movement in onshore regions.[33]

Granular bainite is only found in low-carbon (e.g., 0.15 wt%C) steels and can contain M/A constituents.[20] Unlike upper or lower bainite, granular bainite generally lacks carbides and faceted lath morphology due to having a higher start transformation temperature followed by gradual transformation during continuous cooling of hypoeutectoid steels.[32,34] Although low-angle grain boundaries (LAGB) were observed to separate the laths in both granular bainite and bainitic ferrite, Sun et al.[35] observed an irregular lath morphology in granular bainitic ferrite compared to that of a bainitic ferrite, as shown in **Figure 2**. Furthermore, the ferrite within the granular bainite would have a lower dislocation density compared to upper or lower bainitic ferrite, as shown in Figure 2.[35]

For example, Shimamura et al.[36] observed that when there was higher proportion of granular bainite compared to lath
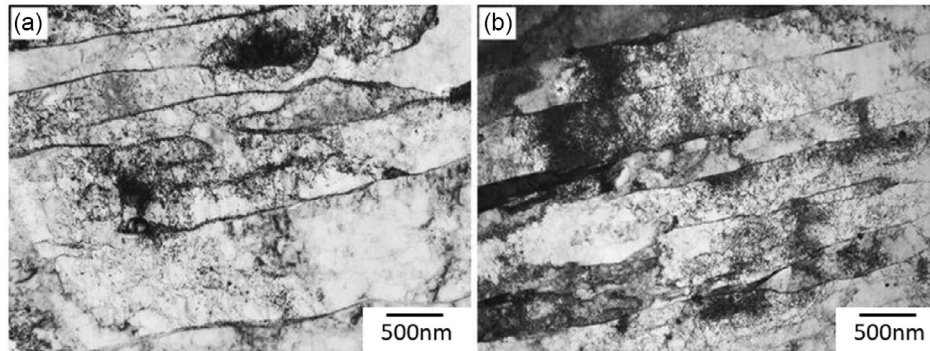
Figure 2. Transmission electron microscopy (TEM) micrographs showing the difference in lath morphologies between a) granular bainitic ferrite and b) bainitic ferrite. Reproduced with permission.[35] Copyright 2014, SpringerNature.

bainite within 0.25 mm below the surface of X65 grade TMCP steel, the hardness decreased to less than 250 HV0.1, increasing the resistance of SSC between the H_2S partial pressure of 0.13–16 bar. This is because increased dislocation density also leads to the higher stress concentration at the tip of corrosion pit which contributes to the increased localization of hydrogen at the tip. This in turns leads to increased susceptibility to hydrogen embrittlement (HE), which results in crack initiation at the tip of the corrosion pit.[37] For example, pipeline steels consisting mainly of granular bainite have been observed to result in at least 1.25 times higher density of corrosion pits compared to that of lath bainite when exposed to low H_2S partial pressure of 0.15 bar. However, the same experiment also revealed that cracks were observed at the tip of the corrosion pit in the microstructure consisting mainly of lath bainite but not that of granular bainite.[37]

Zhang and Kelly[38] observed that granular bainite has a similar crystallographic structure as martensite and suggested that a displacive transformation for granular bainite is involved. The lack of carbides in granular bainite also reduces the need for alloying elements such as Si or Al which acts to stabilize surrounding austenite and inhibit the precipitation of cementite which can act as hydrogen sinks that may contribute to HE.[39] Decreasing the cooling rate increases the partition of carbon from ferrite, increasing the size of granular bainitic ferrite matrix within the granular bainite while reducing the M/A constituents.[40] However, increasing the concentration of carbon within austenite would also reduce the cooling rate needed for the formation of martensite due to saturation of soluble carbon in the surrounding austenite.[20] Thus, granular bainite consists of ferrite matrix and fine M/A constituents as it is difficult to completely avoid the formation of M/A in high-strength steel and bainitic steel TMCP.[41]

Although there has now been a clearer understanding of the transformation mechanism and structure of upper and lower bainite, the structure of granular bainite still remains unclear. There are two schools of thought regarding the structure of granular bainite. On the one hand, granular bainite is regarded as a bainite which undergoes significant recovery resulting in coarse parallel and granular sheaves of bainitic ferrite where TEM observations of the coarse sheaves reveal fine ferrite platelets.[42,43] On the other hand, granular bainite was observed as a matrix of blocky or equiaxed bainitic ferrite consisting carbon-enriched M/A islands.[20,44] Note that this can contribute to the increase

in propagation rate of SSC as less energy will be required to propagate through granular bainite, unlike lath-like bainite due to less obstacles in deviating cracks, as shown in **Figure 3**.[45]

Nevertheless, Li et al.[46] observed a granular bainite structure in the TEM and concluded that the microstructure constitutes both ferrite platelets and equiaxed ferrite matrix with intergranular M/A islands within the same material. This is further supported by Qiao et al.[44] who proceeded to propose two ferrite growth mechanisms during the formation of granular bainite–equiaxial growth and merge of laths, as shown in **Figure 4**. As the transformation temperature decreases, the longer cooling duration allowed for the growth of lath ferrite rather than equiaxed ferrite as the carbon-enriched regions of RA decreased, as shown in Figure 4b.[44] These laths formed are usually wider than upper bainite and separated by rod-like RA compared to that in Figure 4a, increasing the hardness of material.[44]

2.1.3. Quasipolygonal Ferrite

Similar to polygonal ferrite, quasipolygonal ferrite nucleates at PAG boundaries but has a start transformation temperature slightly below that of polygonal ferrite, leading to an irregular and anisotropic morphology.[47] These phenomena are due to elemental partitioning at the growing interface.[48] When comparing between granular bainite and quasipolygonal ferrite, Suikkanen et al.[49] noted the absence of M/A islands in quasipolygonal ferrite. However, it was also found that quasipolygonal ferrite has a higher density of dislocations, MA islands, and hardness than in polygonal ferrite.[50,51] This is further confirmed by Tian et al.[52] who noted the presence of M/A within quasipolygonal ferrite when observed under TEM, as shown in **Figure 5**. Hence, careful characterization is needed as quasipolygonal ferrite and granular bainite can look similar when observed under low magnification due to the irregularities and presence of M/A islands.[53,54] A destructive method in differentiating between quasipolygonal ferrite and granular bainite is by etching.[49,55]

2.1.4. Acicular Ferrite and Widmanstätten Ferrite

Similar to granular bainite, M/A can also form at the boundaries of acicular ferrite.[56] According to Thewlis et al.,[57] ferrite is a mixture of intragranular secondary Widmanstätten ferrite,
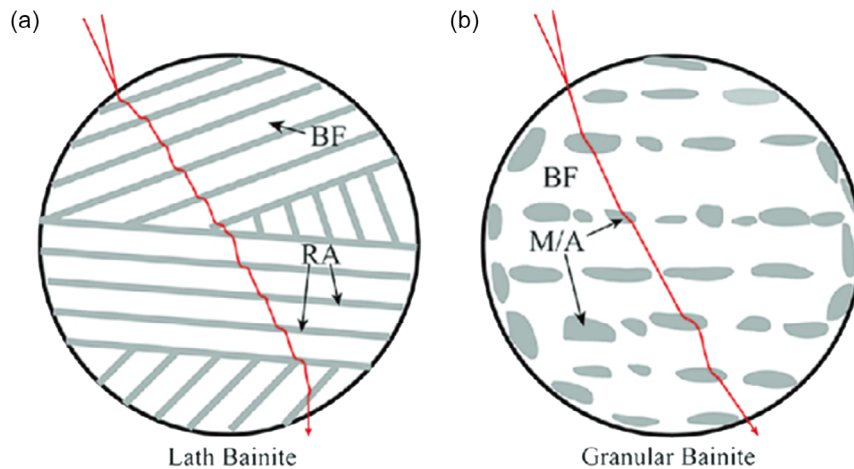
**ADVANCED
SCIENCE NEWS**

www.advancedsciencenews.com

**ADVANCED
ENGINEERING
MATERIALS**

www.aem-journal.com

Figure 3. Schematic diagram showing crack propagation (the crack is indicated by a red line) through different microstructures: a) lath-like bainite which consists of BF and RA films compared to b) granular bainite containing BF and martensite–RA (M/A) islands. Reproduced with permission.[45] Copyright 2019, SpringerNature.
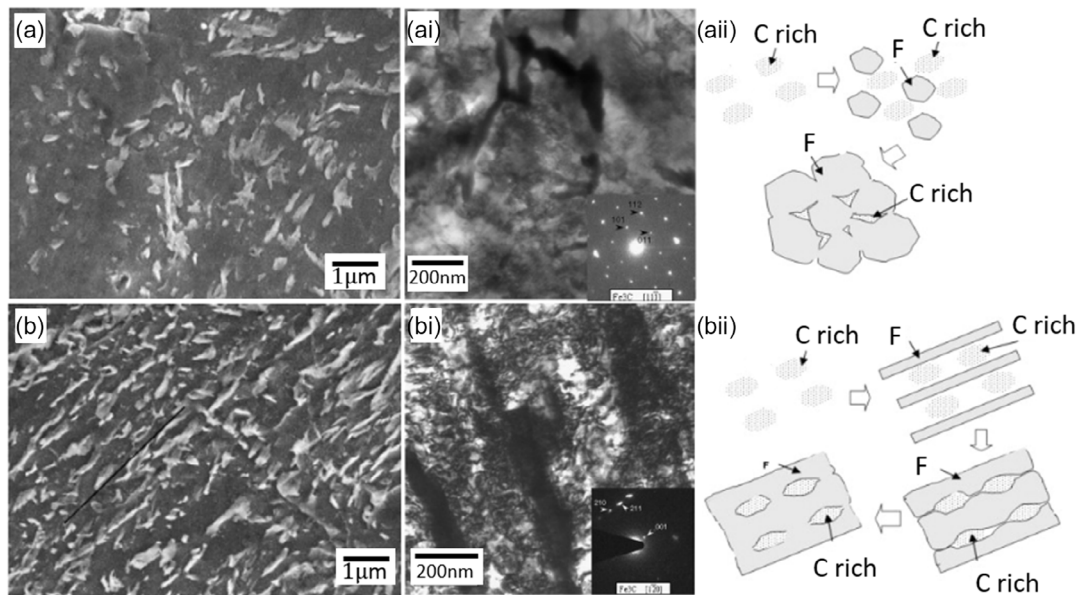

Figure 4. Scanning electron microscope (SEM) micrographs of two different granular bainite morphology; a) equiaxed ferrite and b) ferrite laths. TEM images of the secondary phase observed within (a,b) are shown in ai,bi) while the schematic diagram of the respective transformation process is shown in aii,bii) for the respective granular bainite morphology. Reproduced with permission.[44] Copyright 2009, Elsevier B.V.

idiomorphic ferrite, and intragranular bainite, all of which can coexist in the same microstructure especially under continuous cooling conditions.

On the other hand, Xiao et al.[58] considered acicular ferrite in pipeline steels as a complex mixture of quasipolygonal ferrite, granular bainite, bainitic ferrite, and islands of M/A in a low-carbon Mn–Mo–Nb steel system that can be produced from a wide range of cooling rates, making it ideal for promoting a good combination of strength and toughness in steel.

Yet, Bhadhesia et al.[20] noticed that acicular ferrite also nucleates intragranularly from interfaces between inclusions and surrounding prior austenite matrix. Thus, the nucleation

of acicular ferrite can be at the expense of bainite when the PAG is large enough especially near heat-affected zones of welds.[20] Furthermore, inhomogenously distributed nonmetallic inclusions such as TiN particles surrounded by films of MnS may not only act as sites of irreversible hydrogen traps but also promote acicular ferrite nucleation.[59,60] As such, acicular ferrite may or may not have a specific orientation relationship with the prior austenite as it depends on the crystallographic orientation of the inclusion from which it nucleates.[20]

When analyzing the misorientation angles within acicular ferrite, Shrestha et al.[61] observed that there were high-angle grain boundary (HAGB) peaks at 50–60°. On the other hand, when
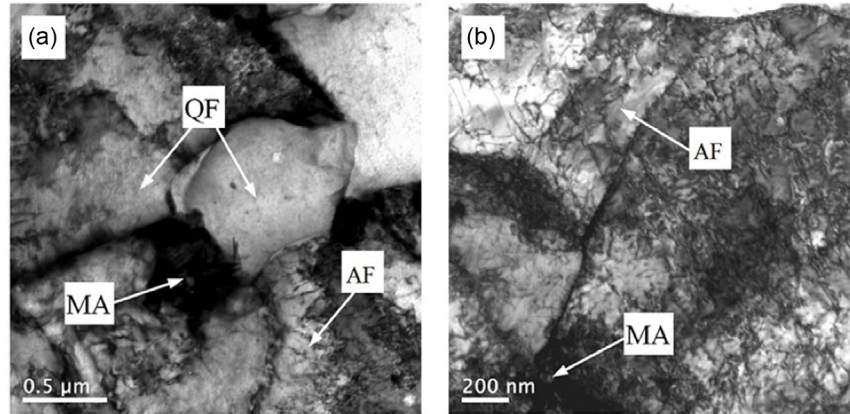
Figure 5. TEM micrograph showing high dislocation density in M/A islands within a) quasipolygonal ferrite and b) acicular ferrite in low-carbon steel produced from ultrafast cooling. Reproduced under terms of the CC-BY license.[52] Copyright 2017, Associação Brasileira de Metalurgia e Materiais - ABM; Associação Brasileira de Cerâmica - ABC; and Associação Brasileira de Polímeros ABPol'.

observing an isothermally cooled low-carbon steel of 0.05 wt%, Kim et al.[62] discovered that the boundaries between substructures within acicular ferrite were ≈1–2° disorientation angles while that of the acicular ferrite grain boundary was at ≈7°. This further supports that acicular ferrite consists of many different types of intergranular and intragranular ferrite with acicular or needle-like structure.

There are two main types of Widmanstätten ferrite: primary Widmanstätten which nucleates from PAG boundaries or from inclusions and secondary Widmanstätten ferrite which nucleates from allotriomorphic ferrite boundaries or idiomorphic ferrite, as shown in **Figure 6**.[57] As the number of inclusions within the parent austenite grain increases, the interlocking and impingement of secondary Widmanstätten ferrite occur,
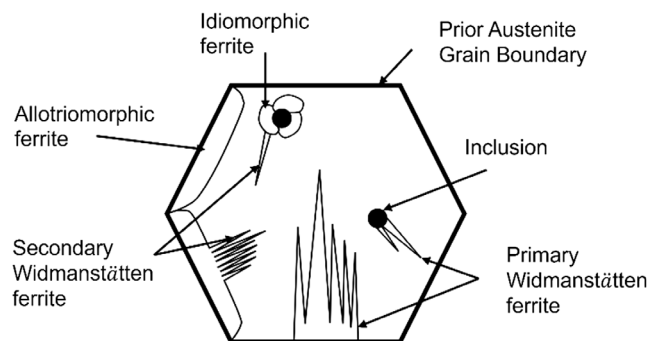
resulting in the formation of a type of acicular ferrite termed as Widmanstätten acicular ferrite.[57] Widmanstätten acicular ferrite forms through the paraequilibrium mechanism, whereby only interstitial (e.g., carbon) instead of substitutional atoms diffuse through the advancing interface of Widmanstätten ferrite during displacive transformation.[57] Although both Widmanstätten ferrite and upper bainite involve deformation through invariant-plane strain, Widmanstätten ferrite grows in pairs of self-accommodating plates to reduce the free energy required for its transformation to a lower level compared to bainite, resulting in coarser plates with lower dislocation density.[20]

The effect of different types of microstructural mixtures discussed are summarized in **Table 1**. When comparing between microstructure consisting mainly of lath and granular bainite, the lower dislocation density in granular bainite results in lower hydrogen trap sites, which lead to higher SSC resistance.[36,37] But overall, the microstructure consisting mainly of acicular ferrite mixture has a lower efficiency as a hydrogen trap site, leading to a higher SSC resistance when compared to those of mainly bainite or pearlite. This is mainly due to the higher fraction of cementite present in bainite and pearlite as compared to acicular ferrite mixture.[63]

Figure 6. Schematic showing different forms of Widmanstätten ferrite. Adapted from.[57] Copyright 2013, Taylor and Francis.

2.2. Local Hard Zones

Recently, local hard zones (LHZs) have been observed in TMCP pipeline steels and were suspected to have led to occurrence of SSC when exposed to highly severe H_2S Region 3 environment defined by ISO 15 156-2.[7,8] According to a series of postmortem

Table 1. Summarized correlation between Microstructural features and SSC resistance as well as hydrogen uptake.

Apparent hydrogen uptake		SSC resistance	
Lath bainite + granular bainite is less than ferrite + pearlite	[131]	Ferrite + bainite is greater than ferrite + pearlite	[132]
Quasipolygonal ferrite + acicular ferrite is less than quasipolygonal ferrite + bainite	[133]	Granular bainite is greater than lath bainite	[36,37]
Ferrite + acicular ferrite is less than ferrite + bainite	[63]	Ferrite + acicular ferrite is greater than ferrite + bainite	[63,134]
		Acicular ferrite is greater than ferrite + pearlite	[135]

ASTM E384 standard microhardness tests of four-point bent samples which were exposed to NACE MR0175 solution, LHZs were observed to mostly contain lath bainite near the surface of TMCP parent material.[64] However, due to the minimum diagonal width of microindentations (e.g., 20 μm as stated by ASTM E384 for Vickers hardness scale), it is difficult to identify these LHZs reliably as they appear inconsistently and exist as inhomogeneous thin layers (less than 500 μm) on the edge, often mistakenly removed during sample preparation. This led to the development of modified qualification procedures with the aim of evaluating SSC within regions of possible LHZ formation.[65]

Fairchild et al.[66] attributed the formation of LHZs to the significant increase of cooling rate to five times beyond that intended for formation of granular bainite all because of a slight difference in oxide film formed during the thermomechanical rolling process of TMCP. For example, it has been observed that the increase in cooling rate of the surface layer of X65-graded pipeline steel to beyond $200\,°C\,s^{-1}$ results in a microstructure which consists mainly of lath bainite. This led to the increase in surface hardness to beyond the critical hardness for the formation of SSC, even when the steel is exposed to H_2S partial pressure of as low as 0.13 bar.[67] Thus, based on the other conventional mechanisms proposed by Fairchild et al, it can be said that LHZs are more likely formed during the TMCP process rather than the deformation of steel slabs into cylinder pipes.[66]

2.3. Role of Reversible and Irreversible Hydrogen Trap Sites on HE

A critical localized hydrogen concentration, which is highly dependent on the nature of hydrogen trap, is required for HE to proceed. In general, the critical trap binding energy of $60\,kJ\,mol^{-1}$ is commonly used to differentiate the lower-hydrogen-affinity reversible traps from the irreversible traps at room temperature conditions.[68–70] At a sufficiently high temperature or heating rate, hydrogen can be released from irreversible traps, and this acts as the underlying concept for various hydrogen measurement techniques in steel. A review of these techniques can be found elsewhere.[71] Examples of reversible traps are edge and screw dislocations, twins, interstitial lattice sites, whereas irreversible hydrogen traps are lattice vacancies, precipitates, and nonmetallic inclusions.[72,73] **Figure 7** shows the types of traps within a TMCP steel.

It must be noted that not all hydrogen trapped within the microstructure contributes toward HE.[74] Hydrogen within reversible traps is normally considered as more detrimental than that in the irreversible traps due to the higher diffusivity, leading to a higher tendency to achieve critical hydrogen concentration in other localized regions.[71,74] Giarola et al.[75] suggested that the increase in bainitic structure, and hence irreversible trap sites, was responsible for decrease in susceptibility to HE. Furthermore, Carrasco et al.[76] also observed that the duration for crack initiation and growth is higher when microstructure consists of irreversible trap sites compared to that which consists of reversible trap sites. Similarly, the increase in irreversible traps like precipitates helps to draw hydrogen away from dislocations within the microstructure, reducing localized
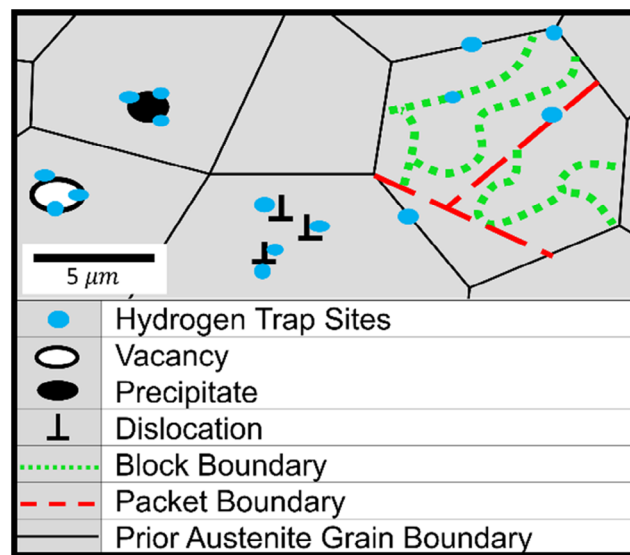

Figure 7. Schematic diagram showing types of hydrogen traps within a TMCP steel microstructure. Adapted from.[129] Copyright 2013, DECHEMA Gesellschaft für Chemische Technik und Biotechnologie e.V.

plasticity.[77] However, this is provided that the irreversible traps sites are not completely filled and are homogenously distributed.[77]

The types of crystal structure within the microstructure can also determine the solubility of hydrogen within the material, leading to different hydrogen content and consequently influencing the susceptibility to SSC within the microstructure. The diffusion coefficient of hydrogen in BCC crystal is higher compared to FCC and hexagonal-close-packed (HCP) crystal structure.[78] Moreover, the diffusion coefficient of hydrogen in austenite is lower than that in ferrite at the same temperature.[74] This is because the hydrogen dissolution energy for the preferable octahedral sites in austenite is lower than the preferable tetrahedral site, leading to a higher hydrogen solubility in austenite than ferrite.[79]

Sun et al.[19] proposed that the relationship between the size of grain boundaries and the density of hydrogen traps (N) can be equated using (Equation (1))

$$N = \frac{nS_G x_{GB}}{2nV_G x_a^3} \tag{1}$$

where: n is the number of grains counted per m^3 and S_G and V_G are the surface area and volume of a grain; the width of grain boundaries (x_{GB}) such as PAG, packets, blocks, and laths can be assumed to be 10 times the distance between two atoms (x_a); the ratio between the dislocation density (ρ_{Dis}) and x_a was assumed to be 5:1 for the same N in the same microstructure.[19] In light of this, Bai et al.[80] suggested that smaller grains would have less dislocation pile-up when compared to larger grains, therefore reducing localized accumulation of hydrogen concentration at grain boundaries.

Additionally, HE susceptibility is also dependent on the disorientation angle at grain boundaries. When the hydrogen

**ADVANCED
SCIENCE NEWS**

www.advancedsciencenews.com

**ADVANCED
ENGINEERING
MATERIALS**

www.aem-journal.com

binding energy of these boundaries was measured, Nagao et al.[81] discovered that PAG, packets, and blocks have approximate values of 57 kJ mol^{-1} unlike that of the lath boundaries approximated to 26 kJ mol^{-1}. This is because PAG, packets, and blocks are considered as HAGBs while lath boundaries are considered as LAGBs.[82,83] The threshold disorientation angle for differentiating between LAGB to HAGB is generally accepted to be 15° based on evaluation of a plot of grain boundary energy against misorientation.[84,85] Thus, different boundaries within the martensitic microstructure will have a different effect in the accumulation of hydrogen and subsequently the behavior of SSC within the microstructure. For example, Masoumi et al.[86] suggested that the increase in HAGB promotes the susceptibility of material to SSC due to the rise in stored energy which subsequently leads to higher number of hydrogen trap sites. On the other hand, Echaniz et al.[87] suggested that HAGB plays an important role in inhibiting the propagation of SSC. Furthermore, decreasing the packet size in a martensitic steel delays the propagation of initiated cracks to reach a critical size through crack deflection and retardation, resulting in reduced threshold stress intensity factor.[88]

3. Environmental Factors Influencing SSC

Environmentally assisted cracks (EAC) can affect the use of alloys in service, especially in environments where there can be an ingress of hydrogen. However, in the presence of applied stress, stress corrosion cracking (SCC) occurs. SSC is hence a specific type of SCC that is limited to the presence of sulfide species from the low-pH aqueous H$_2$S environment of which the steel pipeline is exposed to in operation. As such, both processes of anodic dissolution and cathodic HE contribute to the initiation and propagation of SSC.

3.1. Transition from Anodic Dissolution to HE

When compared between TMCP to direct-quenched or quenched and tempered steel with microstructures of similar PAG size, experiments have shown that TMCP steels were more prone to anodic dissolution but less prone to HE compared to the latter two.[10] This was mainly due to TMCP consisting of the lowest proportion of HAGBs and consequently lowest density of hydrogen trap sites, while having highest amount of dislocation density and consequently highest corrosion current density.[10] Hence, it is important to consider the variables which determine the dominating mechanisms of SSC, that is either anodic dissolution process or HE.

Dunlop[89] observed that the applied cathodic polarization was able to inhibit the propagation of cracks in steel formed in environment containing low 0.01 atmospheric partial pressure of H$_2$S. Thus, Yamane et al.[6] proposed a model for SSC whereby initiation stage of SSC was dominated by localized anodic dissolution at the tip of the corrosion pit followed by HE as the dominant mechanism during the propagation stage of SSC.[37] Based on this proposed model, Samusawa et al.[90] also went on to analyze the depth of corrosion pit within pipeline steels exposed to 0.15 bar H$_2$S partial pressure under different applied stress and concluded that the increase in stress concentration increases the dislocation density and thus the corrosion rate, therefore increasing the depth of corrosion pit. This in turn further increases the localized stress concentration which promotes HE.[90]

Some studies have also shown a threshold potential at which HE will dominate over the anodic dissolution process in facilitating crack growth rate in samples electrochemically charged with hydrogen.[10,11] In order to identify the dominating mechanisms, a common method involves carrying out linear sweep voltammetry of the metal–electrolyte electrochemical system at different rates to identify the regions of anodic dissolution, cathodic HE, or a mixture of both within the polarization curve at which SSC crack propagates.[10,11] Using this method, Liu et al.[11] observed the initial rise in yield strength of X70 grade pipeline steel before decreasing when cathodic potential exceeds -920 mV$_{SCE}$ in a near-neutral pH NS4 electrolyte at ambient temperature. Liu et al.[11] aKributed this phenomenon to the impingement of dislocaBons at the crack Bp by hydrogen when at a lower concentraBon before it transiBons to promote dislocaBon mobility through the HELP mechanism as the concentraBon of hydrogen conBnues to increase.[91] As such, the author attributes the propagation of cracks when hardening effect occurs below a critical hydrogen concentration to anodic dissolution as the dominating mechanism.

3.2. High-Pressure Aqueous H$_2$S

3.2.1. Role of H$_2$S and Hydrogen Recombinant Poison

In an aqueous environment, surface-adsorbed hydrogen atoms are formed through two main mechanisms, which contribute to the Volmer reaction: the reduction of water and the reduction of dissociated protons from H$_2$S.[92]

The majority of the adsorbed hydrogen which formed Fe—H bonds on the surface of steel would then recombine and escape through either the Tafel reaction or Heyrovsky reaction to complete the hydrogen evolution reaction (HER) process.[92] This is often observed in the form of effervescence on the metal surface. However, the presence of sulfide species inhibits the recombination process, thus promoting the absorption of hydrogen which would then diffuse into the bulk. This embrittles the steel and when under applied load, cracks initiate and propagate. This process can be summarized in **Figure 8**.

Iofa and Kam[93] suggested that the bisulphide anion, HS$^-$, from H$_2$S is responsible for accelerating proton discharge and thus promoting adsorption of hydrogen. However, Kawashima et al.[94] discovered that the concentration of H$_2$S remains higher than its dissociated counterpart, and this can be explained by the formation of an unstable complex compound between adsorbed H$_2$S and adsorbed H$^+$, inhibiting the formation of H$_2$ gas. On the other hand, Bockris et al.[95] suggested that H$_2$S lowers the binding energy of Fe–H, which in turn increases the overpotential of hydrogen. Thus, although the exact mechanism has not yet been confirmed, the common understanding is that H$_2$S acts as a hydrogen recombinant poison in the corrosion process. Therefore, it can be understood that using hydrogen recombinant poison in electrolyte would give a more representative charging condition to that in-service.
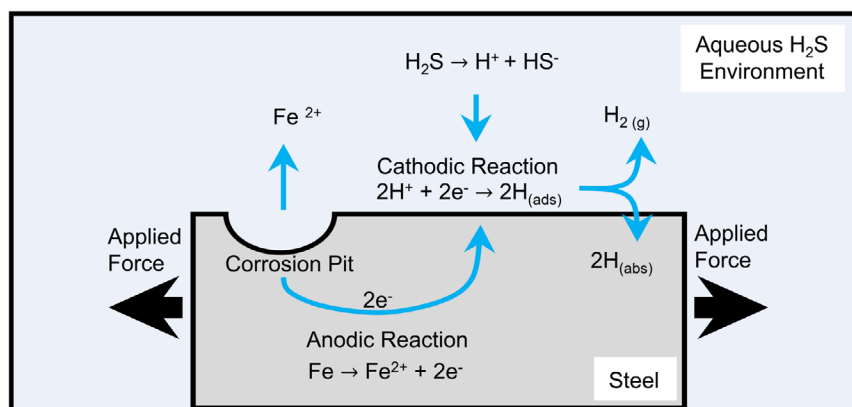
**ADVANCED
SCIENCE NEWS**

www.advancedsciencenews.com

**ADVANCED
ENGINEERING
MATERIALS**

www.aem-journal.com

Figure 8. Schematic showing hydrogen absorption process in steel within aqueous H_2S environment. Adapted from.[130] Copyright 2014, Elsevier B.V.

3.2.2. Effect of Partial Pressure of H_2S and pH on HE

It is known that aqueous H_2S environment accelerates dissolution of steel through the formation of thermodynamically stable iron sulfide layer.[96] Depending on the pH of the environment, the types of corrosion product formed will affect the adsorption of hydrogen differently.[97]

As the concentration of H_2S increases, the dominant corrosion product formed transitions from mackinawite (FeS) and cubic iron sulfide (FeS) to pyrrhotite ($Fe_{1-x}S(x = 0$ to $0.17)$) and troilite (FeS) and even pyrite (FeS_2).[98] When comparing between TMCP steels that consist of pearlite against that of bainite, Marchebois et al.[99] observed a homogenously thicker FeS layer formed on pearlite unlike those on bainite, which were discontinuous and porous due to the lower carbon content in bainite. Zheng et al.[100] discovered that the mixture of mackinawite and pyrrhotite corrosion product layer formed on the surface gave better protection against hydrogen permeation compared to that formed at room temperature. On the other hand, Folena and Ponciano[101] suggested that not only did the formation of pyrrhotite not contribute to the barrier effect, it also reduces the efficiency of the barrier effect. This is because mackinawite layer would need to be ruptured to expose fresh steel surface for pyrrhotite film to form, simultaneously forming a pathway for hydrogen ingress.[101,102] In the same way, a sufficient amount of external force that deforms the material will cause rupture of the corrosion layers formed, revealing the bare steel beneath which favors formation of corrosion pits and reintroducing hydrogen adsorption.

Huang et al.[96] observed that when a mixture of crystalline FeS and mackinawite is formed as corrosion layer, this layer acts as an n-type semiconductor that attracts the S^{2-} and HS^- anions while repelling H^+ cations, reducing the diffusion of H^+ ions to the surface of steel which in turn reduces the reduction of H^+ to form adsorbed H atoms. This further confirms the observations from Wallaert et al.,[103] where the amount of diffusible hydrogen measured from the sample immersed in NACE solution A saturated with H_2S at pH 4 and room temperature rapidly increases to a peak before decreasing less rapidly even though the corrosion rate increases continuously over time. Zhou et al.[104] also observed a similar trend in steel sample-immersed partial pressure of H_2S (pH_2S) of 1 MPa but when compared to that of 0.1 MPa, the peak value for hydrogen permeability was lower peak and a plateau was observed instead of a decay. The higher peak value was because of the twofold mechanism, whereby the increase in pH_2S promotes the cathodic reduction to form H^+ ions and increases the production of HS^- ion that hinders evolution of H_2.[104] As for the plateau, this was possibly due to the much thinner sulfide film formed at lower partial pressure of H_2S, which resulted in a less significant barrier effect in hydrogen permeability.[104]

3.2.3. Effect of the Temperature of H_2S Environment on HE

Temperature also plays a role in the rate of hydrogen activity within the H_2S–H_2O–Fe system. When temperature increases from 298.15 K to 353.15 K at a fixed partial pressure of H_2S of 1 MPa, the corrosion rate generally decreases due to the increase in the amount of S and compactness of sulfide layers formed.[105,106] This in turn decreases the hydrogen permeation flux despite increasing the diffusivity of hydrogen through the material.[100] However, this statement is the opposite from work done by Wang et al.,[107] which shows increasing hydrogen permeation flux as temperature increases from 303.15 to 313.15 K, when partial pressure of H_2S was fixed at 0.1 MPa. A possible reason for this disagreement is the insufficient temperature range performed by Wang et al. Furthermore, the decrease in permeation flux from increase in temperature may also have an opposite effect on the H_2S–H_2O–Fe system, in that hydrogen initially absorbed into bulk of material gets trapped within the material. Moreover, the increase in temperature up to a certain degree promotes diffusion of hydrogen from reversible trap sites to irreversible trap sites within the microstructure. The mechanical performance of the material in this system then depends on which types of hydrogen trap sites, that is, irreversible or reversible, are filled or emptied at different temperatures as well as their relative location to defects within the lattice of the material.

4. Fracture Mechanisms in SSC

SSC is caused by the addition of stress, on top of exposure of a material with a susceptible microstructure to a higher risk

**ADVANCED
SCIENCE NEWS**

www.advancedsciencenews.com

**ADVANCED
ENGINEERING
MATERIALS**

www.aem-journal.com

environment. The stress state on the parent material of a pipeline is complex and there are two origins of note.

4.1. Residual Stresses

These can originate from the deformation process during the manufacturing stage such expansion of the pipe during the UOE process to achieve the desired dimension and inhomogeneous flow of material during cold drawing of seamless pipe.[14,108] Additionally, the bending stress exerted unto pipelines during laying and installation process can also act as a source of residual stress.[109] These residual stress can individually or collectively contribute to the mean stress and subsequently affect the high-cycle-fatigue performance of the pipeline especially when subjected to ground movement.[110] Furthermore, the increase in tensile residual stress can reduce the fracture toughness, increasing the susceptibility of material to SSC.[111] However, a suitable amount of compressive residual stress to the surface can also be beneficial in increasing the resistance of material against HE such as in the case of shot peening treatment.[112]

4.2. Hoop Stress

Among the various types of stress components, hoop stress due to internal operating pressure contributes most significantly to the crack formation in steel pipelines.[113] This circumferential stress can manifest in the form of surface or part-through wall cracks, growing in the axial direction of the pipe before transitioning into through wall cracks.[114] If the through-wall crack grows axially in an unstable manner, rupture instead of leak failure may occur resulting in severe impact on human and environmental safety.[115,116]

The combination of these stress states can result in a superposition of stress that may initiate a new crack or propagate an existing crack, and for SSC, this risk is increased as the presence of hydrogen can change the ductility and toughness of steels in an aqueous H_2S sour environment.

4.3. Overview of HE Mechanisms at Crack Tip

The effect of hydrogen on propagation of crack during SSC within TMCP steels can be narrowed down into three commonly known mechanisms, hydrogen-enhanced localized plasticity (HELP), hydrogen-enhanced decohesion (HEDE), and adsorption-induced dislocation emission (AIDE). These mechanisms can occur in combination with one another depending on the interaction of material microstructure with the adsorbed hydrogen. Briefly, HEDE involves the decrease in cohesive bond and chemical potential of the solute in a lattice structure when tensile load is applied.[117,118] This is due to the increase in local hydrogen solubility which promotes the formation of bonds between Fe ions and hydrogen atoms at crack tip when electrons are donated to fill the highest energy-level orbital of Fe.[119,120] On the other hand, HELP is when absorbed hydrogen decreases the projected shear stress from one dislocation to another, in turn lowering the stress required to move a dislocation through obstacles.[121] Finally, the AIDE theory involves adsorbed

hydrogen within the first few layers of atoms at crack tip leading to localized HEDE.[17] This induces dislocation nucleation and emission at crack tip due to HELP, which leads to alternate slip on slip planes intersecting the crack tip and eventually crack propagation.[17] Simultaneously, emission of dislocation increases the strain in the plastic zone, which may result in microvoid formation just ahead of crack tip.[17] The diffusion of emitted dislocations can also result in microvoids nucleated at inclusions or precipitates in bulk of the material away from plastic zone and these may coalesce to advance the crack.[17]

4.4. Fracture Toughness Evaluation of SSC

In order to investigate the susceptibility of material to SSC, a typical damage-tolerance assessment method involves utilizing fracture mechanics approach to determine the critical stress intensity (K_{IC}) parameter from a fracture toughness test under sour environment conditions. Under mode I tensile loading, the increasing stress intensity and hydrostatic stress at the crack tip will increase in local hydrogen solubility and concentration, leading to HE manifested as brittle intergranular fracture.[117,118] However, enhanced plasticity can also occur through HELP mechanism as hydrogen concentration decreases past a threshold value.[122] This is especially the case when a gradient of hydrogen concentration can exist due to barrier effect of sulfide layers formed at the surface of the sample exposed to H_2S environment. Hence, J-integral introduced by Rice[123] is commonly used to account for the elastoplasticity of fracture toughness behavior. For example, Case et al.[124] developed a method to determine J-integral values from notched slow strain rate tensile tests during SSC using the load and extension measured.

4.4.1. Effect of Hydrogen on Plastic Zone Size at Crack Tip

The presence of hydrogen at the vicinity of crack tip has been shown to increase the plastic zone size.[125] This was attributed to the induced dislocation emission from HELP mechanism by hydrogen at the crack tip.[91] On the contrary, when the plastic zone sizes of samples electrochemically charged with hydrogen were measured by Wang et al.,[126] it was observed that the plastic zone size at crack tip formed as a result of HE was smaller than that of anodic dissolution. According to the model proposed by Murakami et al.,[127] this change from softening to hardening effect was because the hydrogen, outside the plastic zone which is trapped in the core of dislocations, would pin the dislocations, leading to an increased yield stress that constricts the size of plastic zone in the vicinity of crack tip. Despite the differences in the commonly used hydrogen charging method, such as cathodic hydrogen charging, in the case of Wang et al.,[126] and gaseous hydrogen charging, in the case of Murakami et al.,[127] it must be noted that the transition from softening effect to hardening effect is not so much a matter of charging method used; rather, it is more likely from the influence of the concentration of hydrogen.[128]

5. Conclusion and Future Opportunities

SSC remains a challenge for the engineering management of pipelines. In this review, we have highlighted the factors

influencing the susceptibility of TMCP steels to SSC through HE from three perspectives including the microstructure constituents of TMCP, the environmental factors, and the fracture mechanism of SSC.

5.1. Microstructure Constituents Influencing SSC

Since HE influences initiation but dominates the propagation of SSC, the effect of TMCP microstructure on SSC has been discussed in relevance to the influence of types of hydrogen trap sites found in certain types of boundaries, crystallographic lattices, and microconstituents found within the microstructure of TMCP pipeline steels. However, not all hydrogen trapped within the microstructure contributes to SSC. Hydrogen within reversible traps is normally considered as more detrimental than that in the irreversible traps due to the higher diffusivity, leading to a higher tendency to achieve critical hydrogen concentration in other localized regions. PAG boundaries have also been known to be susceptible to SSC. The initiation and propagation of SSC at PAG boundaries are not only affected by the size of PAGs and type of element that partitioned to these boundaries, but also the type of microstructure constituent that nucleates from these boundaries.

The main types of microconstituents discussed were the MA, granular bainite, quasipolygonal ferrite, acicular ferrite, and Widmanstätten ferrite. Among these microstructural features, bainitic laths were commonly found in LHZ, which contribute to the initiation and propagation of SSC. However, future work is required to develop an efficient and precise method of identifying LHZs because the formation of this feature is inconsistent and can appear in thin inhomogeneous layers at the edge of TMCP pipeline steels, often being mistakenly removed from sample preparation.

5.2. Environmental Factors Influencing SSC

Pipeline steels within oil and gas applications are commonly exposed to aqueous H_2S environment. The sulfide species from the aqueous H_2S environment can promote the adsorption of hydrogen atoms by preventing the recombination of hydrogen atoms to form hydrogen molecules. SSC is hence a specific type of SCC that is limited to the presence of sulfide species from the low-pH aqueous H_2S environment of which the steel pipeline is exposed to in operation. As such, both processes of anodic dissolution and cathodic HE contribute to the initiation and propagation of SSC.

Various studies have looked into the variables which influence the transition from anodic dissolution-dominating stage to that of HE, but more research is needed to verify the suitability of the methods used in identifying which of these two is the dominant mechanism. Furthermore, future work is needed to develop a quantitative model to determine the threshold between the two dominating mechanisms (i.e., the transition from anodic dissolution to HE mechanism) to better inform the lifetime prediction of TMCP pipeline steels operating in sour environment. Finally, the mechanisms by which the sulfide species hinders the recombination of hydrogen are still not fully understood and future work should investigate the kinetics and thermodynamics in the steps where sulfide species act to hinder the recombination of H^+.

5.3. Fracture Mechanisms in SSC

SSC is caused by the synergy between various stress components and the exposure of a material with a susceptible microstructure to a low-pH environment. The two main types of stress components experienced by the parent material of a pipeline are the residual stress and hoop stress. These stresses can be exerted during different stages, starting from the pipeline manufacturing process to the internal operational fluid pressures. The combination of these stress states may increase the risk of SSC in TMCP pipeline steels through three common HE mechanisms, that is, HELP, HEDE, and AIDE, depending on the response of the microstructure at the vicinity of the crack tip to the presence of hydrogen.

The enhanced plasticity through HELP led to the application of an elastic–plastic fracture mechanics approach in understanding the resistance of SSC propagation by determining the J-integral of the material through fracture toughness test.

Depending on the content of hydrogen at the plastic zone, sharpening or blunting of crack tip can occur. A model has been proposed to reconcile these two conflicting phenomena. However, further work is needed to verify the proposed model through high-resolution characterization such as transmission electron microscopy to provide evidence of the impingement of dislocation by hydrogen.

Conflict of Interest

The authors declare no conflict of interest.

[1] C. Oouchi, T. Ookita, S. Yamamoto, *Tetsu to Hagane* **1981**, *67*, 969.
[2] P. A. Shenton, in *Corrosion 2005*, NACE International, Houston, USA **2005**, p. 05117.
[3] A. Takahashi, H. Ogawa, *ISIJ Int.* **1996**, *36*, 334.

[4] T. Kaneko, M. Takeyama, M. Nakanishi, Y. Sumitomo, A. Ikeda, in *First NACE Middle East Corrosion Conf.*, NACE International, Houston, USA **1979**, pp. 932–954.

[5] R. J. Pargeter, in *Corrosion 2007*, OnePetro **2007** /NACECORR/proceedings-abstract/CORR07/All-CORR07/126560 (accessed: May 2023)

[6] Y. Yamane, N. Totsuka, M. Kimura, T. Kurisu, K. Motoda, Y. Nakai, in *Corrosion 86*, NACE International, Houston, USA **1986**, p. 167/1.

[7] D. Baxter, E. Østby, S. Chong, A. Venås, in *ASME 2018 37th Int. Conf. on Offshore Mechanics and Arctic Engineering - OMAE*, Vol. 4, American Society of Mechanical Engineers Digital Collection, Madrid, Spain **2018**, https://doi.org/10.1115/omae2018-78653.

[8] North Caspian Operating Company, NCOC Sustainibility Report-2015 **2015**, https://www.ncoc.kz/Documents/Sustainability_report_2015_en.pdf

[9] R. A. King, in *Trends in Oil and Gas Corrosion Research and Technologies* (Ed: A. M. El-Sherik), Woodhead Publishing, Cambridge, UK **2017**, pp. 271–294.

[10] J. Jia, Z. Liu, X. Li, C. Du, W. Li, *Mater. Sci. Eng., A* **2021**, *825*, 141854.

[11] Z. Y. Liu, X. G. Li, Y. F. Cheng, *Corros. Sci.* **2012**, *55*, 54.

[12] L. Chen, R. Case, L. Liu, S. Xiang, H. Castaneda, *Corros. Sci.* **2022**, *198*, 110142.

[13] P. Hopkins, in *5th Asian Pacific International Institute of Welding International Congress*, International Institute of Welding (IIW), Genoa Italy **2007**.

[14] M. D. Herynk, S. Kyriakides, A. Onoufriou, H. D. Yun, *Int. J. Mech. Sci.* **2007**, *49*, 533.

[15] R. J. D. Tilley, *Understanding Solids : The Science of Materials*, 2nd ed., Wiley and Sons, Inc., Chichester, UK **2013**, pp. 88–89.

[16] A. Nagao, C. D. Smith, M. Dadfarnia, P. Sofronis, I. M. Robertson, *Procedia Mater. Sci.* **2014**, *3*, 1700.

[17] S. P. Lynch, *Acta Metall.* **1984**, *32*, 79.

[18] B. D. Craig, *Metall. Trans. A* **1982**, *13*, 907.

[19] Y. Sun, Q. Wang, S. Gu, Z. He, Q. Wang, F. Zhang, *Materials* **2018**, *11*, 412.

[20] H. K. D. H. Bhadeshia, *Bainite in Steels: Theory and Practice*, 3rd ed., Maney Publisher, Boca Raton, USA **2015**.

[21] S. Lynch, *Corros. Rev.* **2012**, *30*, 105.

[22] H. F. Lan, L. X. Du, R. D. K. Misra, *Mater. Sci. Eng., A* **2014**, *611*, 194.

[23] H. Bhadeshia, in *International Seminar on Welding of High Strength Pipieline Steels*, Companhia Brasileira de Metalurgia e Mineração and The Minerals, Metals and Materials Society, Araxá, Brazil **2013**, pp. 99–106.

[24] A. Gingell, X. Garat, in *Corrosion 99*, OnePetro, Houston, USA **1999**.

[25] D. H. Shim, T. Lee, J. Lee, H. J. Lee, J. Y. Yoo, C. S. Lee, *Mater. Sci. Eng., A* **2017**, *700*, 473.

[26] D. C. Ramachandran, S. D. Kim, J. Moon, C.-H. Lee, J.-H. Chung, E. Biro, Y.-D. Park, *Mater. Lett.* **2020**, *278*, 128422.

[27] J. Yang, T. S. Wang, B. Zhang, F. C. Zhang, *Scr. Mater.* **2012**, *66*, 363.

[28] Y. Ohmori, H. Ohtani, T. Kunitake, *Trans. Iron Steel Inst. Jpn.* **1971**, *11*, 250.

[29] L. C. D. Fielding, *Mater. Sci. Technol.* **2013**, *29*, 383.

[30] F. Elhigazi, A. Artemev, *Comput. Mater. Sci.* **2019**, *169*, 109079.

[31] Y. Shinohara, T. Hara, E. Tsuru, H. Asahi, Y. Terada, N. Doi, N. Ayukawa, M. Murata, *Proc. of the Int. Offshore and Polar Engineering Conf.*, Inter. Society of Offshore and Polar Engineers, CuperBno, USA **2007**, pp. 2949–2954.

[32] American Petroleum Institute, *API 5L Specification for Line Pipe*, Am Pet Inst. Washington DC, USA **2004**, Forty Four, pp. 1–40. https://doi.org/10.1520/g0154-12a

[33] S. Endo, N. Nakata, *JFE Tech. Rep.* **2015**, 1.

[34] *ASM Handbook- Metallography and Microstructures* (Ed: G. F. Vander Voort), Vol. 9, ASM Handbook Committee, Ohio, USA **2004**.

[35] C. Sun, S. Yang, G. Liu, *Acta Metall. Sin. Engl. Lett.* **2014**, *27*, 436.

[36] J. Shimamura, I. Samusawa, J. Kondo, D. Izumi, N. Ishikawa, in *Corrosion 2021*, Nace Corrosion, Houston, USA **2021**.

[37] J. Shimamura, T. Morikawa, S. Yamasaki, M. Tanaka, *ISIJ Int.* **2022**, *62*, 2095.

[38] M. X. Zhang, P. M. Kelly, *Scr. Mater.* **2002**, *47*, 749.

[39] D. Quidort, Y. J. M. Brechet, *Acta Mater.* **2001**, *49*, 4161.

[40] S. J. Jia, B. Li, Q. Y. Liu, Y. Ren, S. Zhang, H. Gao, *J. Iron Steel Res Int.* **2020**, *27*, 681.

[41] J. L. Xiao, M. J. Hua, A. J. DeArdo, *Mater. Sci. Forum.* **2014**, *783–786*, 704.

[42] L. J. Habrakan, M. Economopoulos, in *Transformation and Hardenability in Steels*, Climax Molybdenum Co., Ann Harbor, USA **1967**, pp. 69–107.

[43] K. Wu, Z. Li, A. M. Guo, X. He, L. Zhang, A. Fang, L. Cheng, *ISIJ Int.* **2006**, *46*, 161.

[44] Z. X. Qiao, Y. C. Liu, L. M. Yu, Z. M. Gao, *J. Alloys Compd.* **2009**, *475*, 560.

[45] X. Chen, F. Wang, C. Li, S. Liu, in *Minerals, Metals and Materials Series*, Springer International Publishing, Cham, Switzerland **2019**, pp. 549–560, https://doi.org/10.1007/978-3-030-05861-6_52.

[46] X. Li, Y. Liu, K. Gan, J. Dong, C. Liu, *Mater. Sci. Eng. A* **2020**, *785*, 139350.

[47] S. S. Ghasemi Banadkouki, D. P. Dunne, *ISIJ Int.* **2006**, *46*, 759.

[48] M. Hillert, *Metall. Trans. A* **1984**, *15 A*, 411.

[49] P. Suikkanen, P. Karjalainen, A. J. DeArdo, *Int. J. Ital. Assoc. Metall.* **2009**, *101*, 41.

[50] H. Zhao, B. P. Wynne, E. J. Palmiere, *J. Mater. Sci.* **2018**, *53*, 3785.

[51] M. Zhou, L. Du, Y. Zhao, X. Liu, *J. Wuhan Univ. Technol. Mater. Sci. Ed.* **2012**, *27*, 252.

[52] Y. Tian, H. T. Wang, Y. Li, Z. D. Wang, G. D. Wang, *Mater. Res.* **2017**, *20*, 853.

[53] D. De-Castro, A. Eres-Castellanos, J. Vivas, F. G. Caballero, D. San-Martín, C. Capdevila, *Mater. Charact.* **2022**, *184*, 111703.

[54] S. Zajac, V. Schwinn, K. H. Tacke, *Mater. Sci. Forum.* **2005**, *500–501*, 387.

[55] W. C. Jeong, *Metall. Mater. Trans. A* **2003**, *34 A*, 2025.

[56] S. Y. Shin, K. J. Woo, B. Hwang, S. Kim, S. Lee, *Metall. Mater. Trans. A* **2009**, *40*, 867.

[57] G. Thewlis, *Mater. Sci. Technol.* **2004**, *20*, 143.

[58] F. Xiao, B. Liao, D. Ren, Y. Shan, K. Yang, *Mater. Charact.* **2005**, *54*, 305.

[59] F. J. Barbaro, P. Krauklis, K. E. Easterling, *Mater. Sci. Technol.* **1989**, *5*, 1057.

[60] Z. Peng, J. Liu, F. Huang, Q. Hu, Z. Cheng, S. Liu, Y. Cheng, *Steel. Res. Int.* **2018**, *89*, 1700566.

[61] S. L. Shrestha, A. J. Breen, P. Trimby, G. Proust, S. P. Ringer, J. M. Cairney, *Ultramicroscopy* **2014**, *137*, 40.

[62] Y. M. Kim, H. Lee, N. J. Kim, *Mater. Sci. Eng., A* **2008**, *478*, 361.

[63] S. U. Koh, J. S. Kim, B. Y. Yang, K. Y. Kim, *Corrosion.* **2004**, *60*, 244.

[64] X. Yue, W. Huang, A. J. Wasson, J. A. Fenske, T. D. Anderson, B. D. Newbury, D. P. Fairchild, in *Corrosion 2020*, OnePetro **2020**, /NACECORR/proceedings-abstract/CORR20/All-CORR20/446001 (accessed: February 2023).

[65] B. D. Newbury, D. P. Fairchild, C. A. Prescott, T. D. Anderson, A. J. Wasson, in *Proc. Int. Conf. Offshore Mech. Arct. Eng. - OMAE*, Vol. 4, **2019**, pp. 1–9.

[66] D. P. Fairchild, B. D. Newbury, T. D. Anderson, N. S. Thirumalai, in *Proc. Int. Conf. Offshore Mech. Arct. Eng - OMAE*, Vol. 4, **2019**, pp. 1–10.

[67] J. Shimamura, D. Izumi, I. Samusawa, S. Igi, *ISIJ Int.* **2022**, *62*, 740.

[68] R. Silverstein, D. Eliezer, E. Tal-Gutelmacher, *J. Alloys Compd.* **2018**, *747*, 511.

[69] I. Maroef, D. L. Olson, M. Eberhart, G. R. Edwards, *Int. Mater. Rev.* **2002**, *47*, 191.

[70] Gibala, R., DeMiglio, D. S., in *Proc. of the Third Inter. Conf. on Effect of Hydrogen on Behavior of Materials* (Eds: I. M. Bernstein, A. W. Thompson), Metallurgical Society of AIME, Pittsburgh, USA **1981**, pp. 113–122.

[71] D. Rudomilova, T. Prošek, G. Luckeneder, *Corros. Rev.* **2018**, *36*, 413.

[72] A. H. M. Krom, A. D. Bakker, *Metall. Mater. Trans. B* **2000**, *31B*, 1475.

[73] G. M. Pressouyre, *Metall. Trans. A* **1979**, *10*, 1571.

[74] H. K. D. H. Bhadeshia, *ISIJ Int.* **2016**, *56*, 24.

[75] J. M. Giarola, J. A. Avila, O. M. Cintho, H. C. Pinto, M. F. de Oliveira, W. W. Bose Filho, *Fatigue Fract. Eng. Mater. Struct.* **2022**, *45*, 3009.

[76] J. P. Carrasco, D. D. Silva Diniz, J. M. Andrade Barbosa, A. A. Silva, M. Antonio dos Santos, *Int. J. Hydrogen Energy* **2019**, *44*, 3230.

[77] A. Nagao, M. L. Martin, M. Dadfarnia, P. Sofronis, I. M. Robertson, *Acta Mater.* **2014**, *74*, 244.

[78] K. Hirata, S. Iikubo, M. Koyama, K. Tsuzaki, H. Ohtani, *Metall. Mater. Trans. A* **2018**, *49*, 5015.

[79] E. J. Song, H. K. D. H. Bhadeshia, D. W. Suh, *Corros. Sci.* **2013**, *77*, 379.

[80] Y. Bai, Y. Momotani, M. C. Chen, A. Shibata, N. Tsuji, *Mater. Sci. Eng. A* **2016**, *651*, 935.

[81] A. Nagao, M. Dadfarnia, B. P. Somerday, P. Sofronis, R. O. Ritchie, *J. Mech. Phys. Solids* **2018**, *112*, 403.

[82] X. P. Ma, L. J. Wang, C. M. Liu, S. V. Subramanian, *Mater. Sci. Eng. A* **2011**, *528*, 6812.

[83] S. Morito, X. Huang, T. Furuhara, T. Maki, N. Hansen, *Acta Mater.* **2006**, *54*, 5323.

[84] W. T. Read, W. Shockley, *Phys. Rev.* **1950**, *78*, 289.

[85] D. G. Brandon, *Acta Metall.* **1966**, *14*, 1479.

[86] M. Masoumi, C. C. Silva, H. F. G. de Abreu, *Corros. Sci.* **2016**, *111*, 121.

[87] G. P. Echaniz, T. E. Perez, C. Pampillo, R. C. Newman, R. P. M. Procter, G. W. Lorimer, in *Corrosion 97*, NACE International, Houston, USA **1997**.

[88] A. Di Schino, G. Porcu, L. Scoppio, M. Longobardo, G. L. Turconi, *Corrosion 2006*, NACE International **2006**.

[89] A. K. Dunlop, *Corrosion* **1978**, *34*, 88.

[90] I. Samusawa, D. Izumi, J. Shimamura, *Mater. Corros.* **2021**, *72*, 1168.

[91] P. Sofronis, Y. Liang, N. Aravas, *Eur. J. Mech. A. Solids* **2001**, *20*, 857.

[92] Y. Taji, A. Zagalskaya, I. Evazzade, S. Watzele, K.-T. Song, S. Xue, C. Schott, B. Garlyyev, V. Alexandrov, E. Gubanova, A. S. Bandarenka, *Nano Mater Sci*. Published online October 29 **2022**, https://doi.org/10.1016/j.nanoms.2022.09.003

[93] Z. A. Iofa, F. L. Kam, *Prot. Met.* **1974**, *10*, 17.

[94] A. Kawashima, K. Hashimoto, S. Shimodaira, *Corrosion* **1976**, *32*, 321.

[95] J. O. Bockris, J. McBreen, L. Nanis, *J. Electrochem. Soc.* **1966**, *112*, 1025.

[96] F. Huang, P. Cheng, X. Y. Zhao, J. Liu, Q. Hu, Y. F. Cheng, *Int. J. Hydrogen Energy* **2017**, *42*, 4561.

[97] J. Ning, Y. Zheng, D. Young, B. Brown, S. Nešić, *Corrosion* **2014**, *70*, 375.

[98] S. N. Smith, E. J. Wright, in *Corrosion 94*, National Association of Corrosion Engineers, Houston, USA **1994**.

[99] H. Marchebois, B. Cowe, T. Cassagne, in *AMPP Annual Conf.*, OnePetro **2022**, p. 17565.

[100] S. Zheng, C. Zhou, P. Wang, C. Chen, L. Chen, *Int. J. Electrochem. Sci.* **2013**, *8*, 2880.

[101] M. C. Folena, J. A da C. Ponciano, *Eng. Fail. Anal.* **2020**, *111*, 104380.

[102] S. Zheng, C. Zhou, X. Chen, L. Zhang, J. Zheng, Y. Zhao, *Int. J. Hydrogen Energy* **2014**, *39*, 13919.

[103] E. Wallaert, T. Depover, I. De Graeve, K. Verbeken, *Metals* **2018**, *8*, 62.

[104] C. Zhou, S. Zheng, C. Chen, G. Lu, *Corros. Sci.* **2013**, *67*, 184.

[105] D. Abayarathna, A. R. Naraghi, S. Wang, in *Corrosion 2005*, National Association of Corrosion Engineers **2005** http://onepetro.org/NACECORR/proceedings-pdf/CORR05/All-CORR05/NACE-05624/1848227/nace-05624.pdf (accessed: October 2022).

[106] X.-H. Li, C.-X. Liu, B. He, C.-T. Lv, Z.-M. Gao, Y.-C. Liu, *J. Iron Steel Res. Int.* **2022**, *29*, 1836.

[107] Z. Wang, M. Liu, M. Lu, L. Zhang, J. Sun, Z. Zhang, X. Tang, *Int. J. Electrochem. Sci.* **2018**, *13*, 915.

[108] T. Pirling, A. Carradò, H. Palkowski, *Procedia Eng.* **2011**, *10*, 3080.

[109] J. Taby, S. K. Aas, F. P. Figueiredo, in *25th National Congress on Maritime Transportation*, Ship& Offshore Construction, Rio de Janeiro, Brazil **2014**.

[110] *Fatigue of Structures and Materials* (Ed: J. Schijve), SpringerNature, Dordt, Netherlands **2009**, pp. 89–104, https://doi.org/10.1007/978-1-4020-6808-9_4.

[111] X. B. Ren, Z. L. Zhang, B. Nyhus, *Eng. Fract. Mech.* **2010**, *77*, 1325.

[112] T. An, S. Li, J. Qu, J. Shi, S. Zhang, L. Chen, S. Zheng, F. Yang, *Int. J. Fatigue* **2019**, *129*, 105235.

[113] Y. F. Cheng, *Stress Corrosion Cracking of Pipelines* (Ed: R. Winston Revie), Wiley & Sons, Inc., Hoboken, USA **2013**, pp. 43–71.

[114] T. Amano, H. Makino, in *Proc. of the Biennial Inter. Pipeline Conf., IPC*, American Society of Mechanical Engineers Digital Collection **2013**, Vol. 3, pp. 219–227, https://doi.org/10.1115/ipc2012-90216.

[115] W. Zhou, W. Xiang, D. Cronin, *Int. J. Press. Vessels Pip.* **2016**, *147*, 1.

[116] L. Harron, *Oil and Gas Pipelines: Integrity and Safety Handbook* (Ed: R. W. Revie), Wiley and Sons, Inc., Hoboken, USA **2015**, pp. 152–153.

[117] J. C. M. Li, R. A. Oriani, L. S. Darken, *Z. Phys. Chem.* **1966**, *49*, 271.

[118] R. A. Oriani, *Ber. Bunsen Ges. Phys. Chem* **1972**, *76*, 848.

[119] T. Boellinghaus, T. Mente, P. Wongpanya, E. Viyanit, E. Steppan, T. Boellinghaus, *Cracking Phenomena in Welds IV*, Vol. 4 (Eds: J. C. Lippold, C. E. Cross), SpringerNature, Cham, Switzerland **2016**, pp. 383–439, https://doi.org/10.1007/978-3-319-28434-7_18.

[120] A. R. Troiano, *Metall. Microstruct. Anal.* **2016**, *5*, 557.

[121] P. Sofronis, H. K. Birnbaum, *J. Mech. Phys. Solids* **1995**, *43*, 49.

[122] S. Taketomi, R. Matsumoto, S. Hagihara, *ISIJ Int.* **2017**, *57*, 2058.

[123] J. R. Rice, *J. Appl. Mech.* **1968**, *35*, 379.

[124] R. Case, M. Gonzalez, in *Corrosion 2018*, OnePetro, Houston, USA **2018**.

[125] J. Zhang, Y. Sheng, H. Yang, W. Ma, X. Jiang, *Eng. Fract. Mech.* **2022**, *270*, 108587.

[126] Z. F. Wang, C. L. Briant, K. S. Kumar, X. J. Wei, J. Li, W. Ke, *Mater. Trans. JIM* **1998**, *39*, 365.

[127] Y. Murakami, T. Kanezaki, Y. Mine, S. Matsuoka, *Metall. Mater. Trans. A* **2008**, *39*, 1327.

[128] Y. Zhao, M.-Y. Seok, I.-C. Choi, Y.-H. Lee, S.-J. Park, U. Ramamurty, J.-Y. Suh, J.-I. Jang, *Scr. Mater.* **2015**, *107*, 46.

[129] F. Vucko, A. Aoufi, C. Bosch, D. Delafosse, in *Eurocorr,* DECHEMA Gesellschaft für Chemische Technik und Biotechnologie e.V., Estoril, Portugal **2013**.

[130] T. V. S. Chong, S. B. Kumar, M. O. Lai, W. L. Loh, *Eng. Fract. Mech.* **2014**, *131*, 485.

[131] H. Ma, H. Tian, J. Xin, Z. Cui, *Materials* **2021**, *14*, 851.

[132] A. A. Kholodnyi, Y. S. Kuznechenko, Y. I. Matrosov, M. V. Il'ichev, D. I. Yusupov, *Metallurgist* **2019**, *63*, 376.

[133] G. T. Park, S. U. Koh, K. Y. Kim, H. G. Jung, *Corros. Sci. Technol.* **2006**, *5*, 117.

[134] B. Beidokhti, A. Dolati, A. H. Koukabi, *Mater. Sci. Eng. A* **2009**, *507*, 167.

[135] M. C. Zhao, Y. Y. Shan, F. R. Xiao, K. Yang, Y. H. Li, *Mater. Lett.* **2002**, *57*, 141.
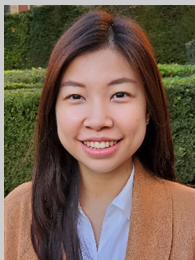
Sarah Hiew Sze Kei is a Ph.D. student at Imperial College London. She received her bachelor's and master's with a year in industry in materials science and engineering at Swansea University where she won Outstanding Academic Achievement Award throughout her undergraduate, year in industry student of the Year, and project management champion. She is currently looking into hydrogen embrittlement and sulfide stress cracking in pipeline steels.

W. M. van Haaften is a senior research engineer of materials and corrosion at Shell, based in Amsterdam. He focuses on material selection for wells, in particular sour wells and wells for hydrogen and CO_2 storage. Before joining Shell in 2012, he started his career at Tata Steel in The Netherlands, working on product development and process improvement of high-strength steels

T. B. Britton (he/him), C.Eng., C.Sci., FIMMM, is an associate professor and associate head of Department (Graduates) in the Department of Materials Engineering at the University of British Columbia and a visiting reader in the Department of Materials at Imperial College London. He leads a research group that focuses on characterizing the interplay of mechanical performance and microstructure in advanced materials used in high-risk high-value applications.

Stella Pedrazzini (she/her) FIMMM is a senior lecturer in Engineering Alloys and Metallurgy at Imperial College London, Engineering and Physical Sciences Research Council (EPSRC), Early Career Fellow, and Royal Academy of Engineering Associate Research Fellow at Imperial College London, UK. She runs a research group on the environmental degradation of engineering alloys, with a particular interest in oxidation and hot corrosion of nickel- and cobalt-based superalloys, aqueous corrosion of steel, as well as advanced characterization techniques such as transmission electron microscopy and atom probe tomography.

© 2023 The Authors. Advanced Engineering Materials published by Wiley-VCH GmbH